AIAA JOURNAL
Vol. 38, No. 8, August 2000

Refined Interaction Method for Direct Numerical Simulation of Transition in Separation Bubbles

Ulrich Maucher,* Ulrich Rist,† and Siegfried Wagner‡
University of Stuttgart, 70550 Stuttgart, Germany

In direct numerical simulations (DNS) of laminar-turbulent transition in laminar separation bubbles, the definition of a well-posed freestream boundary condition is crucial. Different, partially contradicting properties are required: first, an adverse pressure gradient has to be imposed to force separation. Moreover, oscillations at the freestream boundary caused by disturbance waves, which extend into the potential flow, have to be treated accurately. Finally, displacement effects of the separation bubble on the surrounding potential flow by the so-called viscous-inviscid boundary-layer interaction have to be captured. Usually, either the integration domain has to be sufficiently high, or a state-of-the-art boundary-layer interaction model based on the theory of thin airfoils can be applied. At a high Reynolds number at separation, neither possibility is applicable. Therefore, an improved model has been developed that meets the just-mentioned requirements. The method is validated by variations of the height of the integration domain. It is shown that boundary-layer interaction has not only quantitative but even qualitative impact on the separation bubble. The comparison of a highly resolved DNS with an experiment proves the applicability of the present method for separation bubbles on airfoils.

Nomenclature

$\boldsymbol{C}_u$, $c_{u,ij}$ = matrix and its coefficients; Eqs. (15) and (16)
$\boldsymbol{C}_v$, $c_{v,ij}$ = matrix and its coefficients; Eqs. (12) and (13)
c = chord length
c_i = blending function in interaction model
f_c = polynomial function (interaction model)
H_{12} = boundary-layer shape factor
I = total number of discrete sources in the model
L = reference length
Ma = Mach number
n_1, n_2, Δn = index of first and last x station and x increment of the source distribution in the model, respectively
p_w = pressure at the wall
Re = Reynolds number
Re_{δ_1} = Reynolds number based on displacement thickness
q = source distribution in the interaction model
T_{TS} = forcing cycle of the Tollmien–Schlichting (TS) wave
t = time
U_2 = first higher harmonic of TS wave
u, v, w = velocity components in x, y, and z direction, respectively
u_∞ = reference velocity
x, y, z = streamwise, wall-normal, and spanwise coordinate, respectively
x_{ia} = begin of instantaneous update in interaction model
α = streamwise wave number: $\alpha = 2\pi/\lambda_x$
α_e = assumed streamwise wave number at free stream boundary
α^* = assumed total wave number at freestream boundary
γ = spanwise wave number: $\gamma = 2\pi/\lambda_z$
$\tilde{\Delta}$ = modified Laplace operator; Eq. (6)
δ_1 = displacement thickness:
$$\int_0^{y_e} \left(1 - \frac{u}{u_e}\right) \mathrm{d}y$$
δ_2 = momentum thickness:
$$\int_0^{y_e} \frac{u}{u_e}\left(1 - \frac{u}{u_e}\right) \mathrm{d}y$$
ε_{ia} = amplitude limit in interaction model
ξ_{ij} = streamwise distance to a discrete source
ω = vorticity

Subscripts

e = at freestream boundary
i = x station of induced velocity
j = x station of inducing source
k = spanwise spectral mode
p = potential flow
s = at separation
v = caused by viscosity

Superscripts

I = inverse matrix
$\bar{}$ = time-averaged variable
$\hat{}$ = dimensional variable

Received 22 March 1999; revision received 21 October 1999; accepted for publication 22 November 1999.

*Research Assistant, Institut für Aerodynamik und Gasdynamik, Pfaffenwaldring 21.
†Senior Research Scientist, Privatdozent, Fluid Dynamics, Institut für Aerodynamik und Gasdynamik, Pfaffenwaldring 21.
‡Professor, Aero- and Gasdynamics, Institut für Aerodynamik und Gasdynamik, Pfaffenwaldring 21. Member AIAA.

I. Introduction

A BOUNDARY layer subject to a strong adverse pressure gradient is susceptible to separation. In the separated region disturbance waves, so-called Tollmien–Schlichting (TS) waves, are strongly amplified, and transition to turbulence takes place. The increased momentum transfer toward the wall finally forces the boundary layer to reattach. Besides this more general understanding, the physics of laminar separation bubbles (LSB) is still not well understood. Apart from the acceleration of transition and the according higher skin friction, LSBs have a strong impact on the aerodynamic properties of airfoils through the interaction of the boundary layer and the surrounding potential flow, the viscous-inviscid interaction. Displacement effects of the boundary layer can change the potential flow in the separated region or, even worse, around the entire airfoil. A typical pressure plateau is generated near the separated region followed by a sudden pressure increase at the end of the bubble.

As the computers became more powerful, direct numerical simulation (DNS) turned out to be a well-suited tool to investigate the physics of LSBs. On the one hand, DNS can achieve very low (numerical) turbulence to investigate the self-excited behavior of separation bubbles.[1–5] On the other hand, the interaction of special

two- and three-dimensional disturbances is investigated in controlled numerical experiments. Rist[6] and Pauley[7] were the first to perform controlled three-dimensional simulations of the transition in a LSB. Rist and Maucher[8] and Rist et al.[9] continued the work of Gruber, which was restricted to two-dimensional phenomena. By decelerating a Blasius boundary layer to $\approx 91\%$ of the initial velocity, they forced the boundary layer to separate and a separation bubble to form. The Reynolds number based on displacement thickness at separation in these simulations was close to $Re_{\delta_{1,s}} = 1.25 \times 10^3$. Rist et al.[9] forced different combinations of two- and three-dimensional waves upstream of the separation bubble and obtained a strictly convective behavior of all disturbance waves in the investigated test cases. They observe that secondary disturbance amplification is considerably reduced as the amplitude of the two-dimensional TS wave saturates, and transition to turbulence seems not to be caused by secondary instability. Because weakly oblique three-dimensional modes are almost as amplified as clean two-dimensional waves, they suggest that an oblique breakdown mechanism is very likely to occur and to provide the three dimensionality needed for transition to turbulence. The oblique breakdown inherently generates longitudinal vortices. Such vortices observed in DNS and experiments by other authors were usually attributed to Görtler vortices.

If the Reynolds number is further increased to $Re_{\delta_{1,s}} = 2.4 \times 10^3$, Maucher et al.[10] found temporal growth of three-dimensional modes with the presence of a saturated two-dimensional TS wave in the reattachment region (amplitude $\approx 20\% u_\infty$). This temporal growth increases if the separation bubble is bigger especially in terms of the reverse flow intensity. It finally causes transition to turbulence even if the flow is purely two-dimensional upstream of the separation bubble.[11]

Wasistho,[12] Alam and Sandham,[13] and Spalart and Strelets[14] performed DNS focusing on the development of turbulence downstream of the LSB including, however, the whole separation bubble in the integration domain. The Reynolds number in these investigations is $Re_{\delta_{1,s}} \lesssim 1.0 \times 10^3$. Wasistho[12] uses a compressible numerical code at $Ma = 0.2$ and forces a two-dimensional TS wave and a pair of three-dimensional waves with an amplitude of $1\%\ u_\infty$ each. From the observation of a three-dimensionally deformed wave front in terms of spanwise vorticity, which he denotes as Λ shaped, he concludes that Λ vortices are present. Alam and Sandham[13,15] force a pair of symmetrically oblique waves with large amplitude. In their simulation transition is characterized by a staggered pattern of Λ vortices, which might be caused by a bypass mechanism. Spalart and Strelets[14] use a spectral ansatz in streamwise direction, and disturbances propagating into the fringe region are damped. They provide arbitrary two- and three-dimensional disturbances with amplitudes about 5×10^{-4} in the Blasius boundary layer upstream of separation. A flapping of the free shear layer in the front part of the separation bubble is observed, which dominates by far in comparison with convective disturbance waves. Whether the flapping or possible large-amplitude traveling waves cause transition is difficult to answer.

In the numerical schemes mentioned, there are, in general, two approaches to decelerate the boundary layer and thus force separation. The first approach prescribes a wall-normal velocity distribution v_e at the freestream boundary of the integration domain. This is similar to an experimental apparatus, where transition on a flat plate is forced by a displacement body or by suction through the opposite wall in a channel (here denoted as *channel formulation*). This method is used by most of the authors already mentioned. In the second approach, in contrast, based on the work of Gruber and Rist, we prescribe the streamwise velocity component at the freestream u_e and allow for displacement effects by applying a von Neumann boundary condition for the wall-normal velocity component, which is defined according to the equation of continuity ($\partial v/\partial y|_e = -\mathrm{d}u_e/\mathrm{d}x$; x and y are the streamwise and wall-normal coordinates, respectively). This procedure is strongly related to boundary-layer methods and meets the conditions at an airfoil, where a decelerated velocity distribution is forced upon the boundary layer by the inviscid streamwise velocity distribution and where no walls limit displacement in the far-away flowfield (termed *free-flight formulation* later).

Wasistho et al.[16] prescribe the wall-normal distribution obtained in a first simulation with a fixed streamwise u_e distribution (case A) as a wall-normal boundary condition in a second DNS (case B). They show that the results of both DNS (A and B) are equivalent.

Hsiao and Pauley[17] compare results for marginal separation at low Reynolds number obtained by DNS (channel formulation) with a boundary-layer approach, where the viscous-inviscid boundary-layer interaction was taken into account (free-flight formulation). In the DNS a suction port with a fixed suction distribution was inserted into an elsewhere nontranspiration freestream boundary. Even in a very high integration domain separation was strongly delayed in DNS by the displacement of the growing boundary layer, which accelerates the flow in comparison with the boundary layer method caused by a narrowing of the channel. When the nontranspiration condition is replaced by a von Neumann condition for the wall-normal velocity component outside the suction port, Hsiao and Pauley[17] gained favorable agreement with the boundary-layer method (modification toward free-flight condition). On the other hand, this limits the width of the suction port to small streamwise extends.

Spalart and Strelets[14] apply a suction port according to the original boundary condition of Hsiao and Pauley. The flapping of the free shear layer in their DNS might be caused by channel effects, i.e., a strong unsteady widening and narrowing of the effective channel height caused by unsteady displacement effects. If one imagines an experiment in a very low channel with a height of only a few boundary-layer thicknesses, according to typical boxes in DNS it is evident that blockage effects can have strong impact on the streamwise potential velocity component and thus on the pressure distribution, especially if an unsteady separation bubble occurs.

Hildings[18] recalculates an experiment, where separation was forced on a flat plate by a displacement body at the opposing wind-tunnel wall. He prescribes either the measured wall-normal (channel formulation) or streamwise velocity component at the freestream (free-flight formulation) and calculates the respective missing component according to the condition of vanishing spanwise vorticity at the freestream ($\partial u/\partial y|_e = \partial v/\partial x|_e$). Both formulations achieve only coarse qualitative agreement with the experimental findings. The channel formulation cannot guarantee the accurate reproduction of the flow in an experimental channel, if the computational box does not span the entire channel. At the Institut für Aerodynamik und Gasdynamik, Augustin began promising attempts to reproduce the same experiment with our boundary condition (free-flight formulation, von Neumann condition for v), and we feel that the free-flight formulation is superior to the truncated-channel formulation (i.e., where the computational box covers only a smaller part of the experimental channel). However, for reliable statements further research is necessary.

Calculations (with the free-flight formulation) of airfoil separation bubbles show that the velocity distribution at the edge of the boundary layer deviates from the prescribed distribution at the freestream boundary (see later in this paper). A typical velocity distribution with a velocity plateau appears, even if the integration domain covers only a few heights of the boundary layer, because a relaxation of the potential velocity toward the freestream boundary takes place. Actually, this formulation captures the main properties of LSBs on airfoils. The definition of an appropriate boundary condition with the channel formulation, in contrast, is very difficult. The final wall-normal velocity distribution at a specific distance from the airfoil is not known at the beginning of the DNS. It depends significantly on the distance from the wall, especially if a strong streamwise pressure gradient is present. The definition of the boundary condition needs to make assumptions, which in turn have strong impact on the development of the LSB. Prescribing the wall-normal component at the freestream in DNS of airfoil separation bubbles therefore requires a detailed knowledge about the effects of the LSB, whereas prescribing the streamwise component primary rests on the usually a priori known inviscid velocity distribution that finally causes separation. It varies only weakly in wall-normal direction, and the influence of the height of the integration domain on the numerical results is usually smaller. Besides these general differences, the findings of Hsiao and Pauley, as well as our experience, provide evidence of the advantages of a von Neumann condition for the wall-normal velocity component in DNS of airfoil LSB.

For thick boundary layers (large Reynolds number at separation) none of the approaches available so far yields satisfactory solutions for LSB on airfoils. To obtain quantitative findings, the effect of boundary-layer interaction at the freestream boundary cannot be neglected. This problem is addressed in the present paper.

Since the 1970s, strong attempts to model the boundary-layer interaction in numerical schemes were made. Now, viscous-inviscid boundary-layer interaction models are frequently used for boundary-layer calculations in flat integration domains, where the wall-normal extent is very small compared with the streamwise extent. In such models the initially prescribed (inviscid) potential velocity distribution u_p is superposed with a viscous component (index v) caused by the displacement of the boundary layer. The displacement is regarded as a modification of the shape of the wall contour and is modeled with a distribution of sources and sinks $q(x)$ at the wall. The velocity distribution $u(y_e)$ is updated by adding the streamwise velocity component u_v, which is induced by the sources at the wall. Employing the theory of thin airfoils,[19] the sources can be easily calculated[20]:

$$v_v(x) = \frac{\mathrm{d}}{\mathrm{d}x}(u_p \delta_1), \qquad q(x) = \frac{1}{2} v_v(x) \tag{1}$$

where δ_1 denotes the displacement thickness.

Gruber[2] applied such a model to his DNS code for the investigation of two-dimensional instability in LSBs. He shows that the wall-normal viscous velocity component v_v at the freestream boundary is connected to the instantaneous wall-normal value $v(x, y = y_e)$ and an inviscid part v_p:

$$v_v(x) = v(x, y_e) - \int_0^{y_e} \frac{\partial v_p}{\partial y}\,\mathrm{d}y = v(x, y_e) + y_e \frac{\mathrm{d}u_p}{\mathrm{d}x} \tag{2}$$

He tested this method at small Reynolds numbers ($Re_{\delta_{1,s}} \approx 6 \times 10^2$) and obtained reliable results.

Tests with Gruber's model at Reynolds numbers typical for midchord bubbles of glider wing sections or high-lift devices ($Re_{\delta_{1,s}} \approx 2.5 \times 10^3$) failed. At best, only coarse qualitative agreement with the experiment could be obtained. Such simulations demand a tall integration domain (whereas the streamwise discretization necessary to resolve the fine-scale transitional structures is almost unaffected by the Reynolds number). The theory of thin airfoils [which is the basis for Eq. (1)] increasingly overestimates the streamwise viscous component u_v in higher integration domains. Moreover, disturbance waves extend far out into the potential flow and cause oscillations at the upper boundary, which, as a consequence, are modeled as source distribution at the wall. Errors caused by the simplifications in the model (i.e., the displacement is modeled at the wall and not in the boundary layer, where it originates) decay only slowly in the streamwise direction ($\propto 1/x$) compared to TS waves, which might be generated far upstream of the bubble by such errors. Once generated, they are amplified exponentially to such amplitudes that can exceed the amplitude of the initiating errors in the separated region by far, rendering the DNS useless.

Nevertheless, in the DNS of LSBs at high Reynolds numbers there are numerical motivations for the application of an interaction model. Imposing the velocity distribution in a low domain has a very rigid impact on the velocity distribution at the edge of the boundary layer. Displacement effects are mostly suppressed. Very high domains allow for changes of the potential flow in wall-normal direction, and if the height of the integration domain is varied, the edge-velocity distribution therefore changes in spite of similar boundary conditions. A well-defined interaction model has to capture the displacement effects properly, simultaneously avoiding the dependency on the height of the integration domain.

II. Numerical Method

A. Governing Equations

The DNS numerical scheme is based on the complete Navier–Stokes equation for incompressible flow in the vorticity-transport formulation[21,22]

$$\frac{\partial \boldsymbol{\omega}}{\partial t} - \mathrm{rot}(\boldsymbol{v} \times \boldsymbol{\omega}) = \tilde{\Delta}\,\boldsymbol{\omega} \tag{3}$$

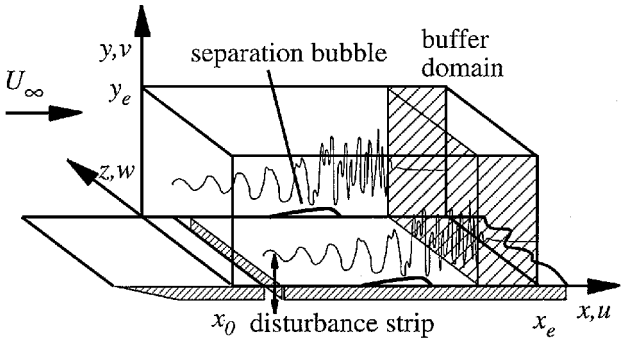

Fig. 1a Integration domain.

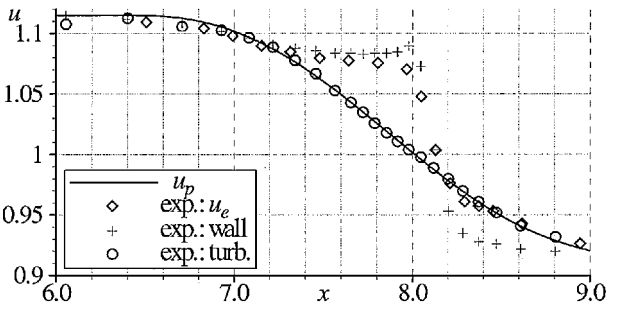

Fig. 1b Velocity distributions in the experiment (symbols) and boundary condition for the DNS (——): $x = 10 \equiv 100\%$ chord length.

with

$$\boldsymbol{\omega} = -\mathrm{rot}\,\boldsymbol{v} \tag{4}$$

which is solved in a rectangular integration domain (Fig. 1a). $\boldsymbol{\omega}$ denotes the vorticity; $\boldsymbol{v} = (u, v, w)$ consists of the velocity components in streamwise (x), wall-normal (y), and spanwise (z) directions, respectively. All variables are nondimensionalized by a reference length $\hat{L}$ and by the velocity $\hat{u}_\infty$. The Reynolds number is $Re = \hat{u}_\infty \hat{L}/\hat{\nu}$, where $\hat{\nu}$ is the kinematic viscosity:

$$x = \hat{x}/\hat{L}, \qquad y = \sqrt{Re}(\hat{y}/\hat{L}), \qquad z = \hat{z}/\hat{L}$$
$$u = \hat{u}/\hat{u}_\infty, \qquad v = \sqrt{Re}(\hat{v}/\hat{u}_\infty), \qquad w = \hat{w}/\hat{u}_\infty \tag{5}$$

Additionally, the wall-normal direction y and the according variables are stretched by $\sqrt{(Re)}$. This leads to a modified Laplace operator:

$$\tilde{\Delta} = \frac{1}{Re}\frac{\partial^2}{\partial x^2} + \frac{\partial^2}{\partial y^2} + \frac{1}{Re}\frac{\partial^2}{\partial z^2} \tag{6}$$

The velocity components are computed from three Poisson equations:

$$\frac{\partial^2 u}{\partial x^2} + \frac{\partial^2 u}{\partial z^2} = -\frac{\partial \omega_y}{\partial z} - \frac{\partial^2 v}{\partial x \partial y} \tag{7}$$

$$\tilde{\Delta} v = \frac{\partial \omega_x}{\partial z} - \frac{\partial \omega_z}{\partial x} \tag{8}$$

$$\frac{\partial^2 w}{\partial x^2} + \frac{\partial^2 w}{\partial z^2} = \frac{\partial \omega_y}{\partial x} - \frac{\partial^2 v}{\partial y \partial z} \tag{9}$$

B. Boundary Conditions and Discretization

In spanwise direction a spectral ansatz is applied, which implies periodic boundary conditions. The equations are solved with a highly efficient, parallelized finite difference method, fourth-order accurate in time (Runge–Kutta) and space. Because of the spectral ansatz in spanwise direction, all equations can be solved independently for each spanwise spectral mode. The Poisson equations for u and w [Eqs. (7) and (9)] even reduce to ordinary differential equations in streamwise direction and lead to pentadiagonal systems.

Only the v equation (8) has to be solved iteratively by a line relaxation method accelerated by a multigrid algorithm. The spectral ansatz allows the specification of different boundary conditions for the two- and three-dimensional part of the flow.

Because the freestream boundary is in the potential flow, the vorticity is set to zero in the vorticity-transport equations. The inviscid streamwise velocity component u_p is prescribed for the two-dimensional part. With the continuity equation

$$\frac{\partial v_p}{\partial y} = -\frac{\partial u_p}{\partial x} \tag{10}$$

an additional condition for v is defined and implemented into the v Poisson equation by means of a compact difference at the freestream including the first wall-normal derivative. It allows for a larger wall-normal velocity component caused by displacement effects even if no interaction model is applied. Moreover, continuity and vanishing vorticity are guaranteed. For the three-dimensional part, exponential decay of the wall-normal velocity is implemented instead of Eq. (10):

$$\frac{\partial v_{3D}}{\partial y} = -\frac{\alpha_k^*}{\sqrt{Re}} v_{3D} \tag{11}$$

where $\alpha_k^* = \sqrt{[\alpha_e^2 + (\gamma_k)^2]}$ denotes an individual wave number specified for each spectral mode k that consists of the respective spanwise wave number γ_k and a streamwise wave number $\alpha_e = \text{const}$ (Ref. 23). In the potential flow this condition is exact for linear TS waves with the streamwise wave number $\alpha_e = \alpha_{TS}$.

At the inflow boundary steady Falkner–Skan profiles or Blasius profiles are prescribed. The three-dimensional part of the flow is set to zero. If controlled conditions are required, disturbance waves can be forced by periodic or pulse-like wall-normal suction and blowing in a disturbance strip at the wall. Except for the disturbance strip, the no-slip condition is applied at the wall.[23]

The unsteady vorticity components are smoothly damped to steady-state values in the buffer domain upstream of the outflow boundary.[22] Consequently, the unsteady velocity components also decay exponentially in the streamwise direction and vanish at the outflow.

C. Boundary-Layer-Interaction Model

The viscous component $v_{v,i}$ is modeled at each Δnth of the total of N streamwise grid points in the limits from n_1 near the inflow boundary to n_2 upstream of the buffer domain at the outflow boundary, resulting in $I = 1 + (n_2 - n_1)/\Delta n$ discrete sources q_j:

$$v_{v,i} = \boldsymbol{C}_v q_j \tag{12}$$

The indices i and j denote the streamwise positions of the viscous velocity component $v_v(x_i)$ and of the source $q(x_j)$, respectively, where $1 \le i, j \le I$. The matrix $\boldsymbol{C}_v$ has the coefficients

$$c_{v,ij} = (1/2\pi)\left[y_e \left| \left(\xi_{ij}^2 + y_e^2\right)\right.\right] \tag{13}$$

where ξ_{ij} denotes the streamwise distance from the source $(x_i - x_j)$ and y_e is the location of the freestream boundary. For large y_e the inviscid theory has to be applied without such assumptions as they are made in the theory of thin airfoils. $\boldsymbol{C}_v$ is inverted once at the beginning of the DNS, giving the relation

$$\boldsymbol{q} = \boldsymbol{C}_v^I \boldsymbol{v}_v \tag{14}$$

Because the matrix $\boldsymbol{C}_v$ is ill conditioned especially in high integration domains and for narrow spacing of the sources, a minimum spacing considerably larger than the streamwise discretization is required ($\Delta n > 1$), which at the same time limits the total number I of sources used. Finally, the streamwise viscous velocity component is calculated at all x stations between n_1 and n_2 out of

$$\boldsymbol{u}_v = \boldsymbol{C}_u \boldsymbol{q} \tag{15}$$

where the $(n_2 - n_1 + 1) \times I$ matrix $\boldsymbol{C}_u$ has the constant coefficients

$$c_{u,ij} = (1/2\pi)\left[\xi_{ij} \left| \left(\xi_{ij}^2 + y_e^2\right)\right.\right] \tag{16}$$

The boundary-layer-interaction model is implemented into the multigrid scheme for solving the two-dimensional part of the v Poisson equation. The boundary conditions of the three-dimensional spanwise spectral modes are not effected. During each multigrid cycle of the two-dimensional v Poisson equation (V cycle with four grids and 2/10/1 iterations on the respective grid after coarsening/on the coarsest grid/after refinement), the von Neumann condition at the freestream boundary is fixed. At the end of the cycle, Eqs. (2), (14), and (15) are calculated to update the von Neumann condition at the freestream boundary of the v Poisson equation:

$$\left.\frac{\partial v}{\partial y}\right|_e = -\frac{\mathrm{d}(u_v + u_p)}{\mathrm{d}x} \tag{17}$$

The interaction model introduces an additional boundary condition at the freestream boundary in addition to vanishing vorticity $\omega_{z,e}$. It turned out that u_v should be adapted with an underrelaxation of 0.55 for optimum convergence. This procedure is only repeated for the first three of a total of eight multigrid cycles, on the one hand, because the variation of u_v stops decaying from one cycle to the next. On the other hand, the convergence rate of the multigrid scheme is much worse when the model is active than without it.

According to the linear stability theory (LST), TS waves do not cause displacement because the displacement of the near-wall maximum is compensated by the reverse effect of the second maximum in the u eigenfunction. Also, the wall-normal velocity component vanishes with increasing distance from the wall and finally approaches zero exponentially [cf. our boundary condition equation (11)]. Because of the finite distance of the freestream boundary from the wall, the model takes into account only the displacement up to the location of the freestream boundary and neglects the rest. Thus, in the model each TS wave has a significant displacement effect. The respective sources and sinks induce oscillations at the entire freestream boundary. However, the mean value of these oscillations is low (for a linear TS wave it is zero). The instantaneous update of the viscous component is very efficient at streamwise stations where the freestream disturbance amplitude is still large compared to the maximum in the boundary layer. In particular, downstream of the LSB even high-frequency displacement effects caused by large-amplitude vortices are captured, and an accurate treatment of such oscillations at the freestream boundary is ensured (see next section). However, strong detrimental upstream influence might be caused by such oscillations because of the model.

In many cases it may be sufficient to apply the model in the way described up to here. However, in our case it turned out that the region upstream of the LSB had to be treated in a special manner in order to suppress TS-like oscillations caused by the problems just mentioned in the model. Because the amplitude of the TS waves almost totally decays toward the freestream boundary, no special boundary condition for disturbance waves is required upstream of the LSB. It is sufficient to just model the influence of displacement effects on the mean flow and its stability properties. Thus, only the temporal development of the mean of the viscous velocity component $\bar{u}_v$ has to be captured in the model. It is calculated in time intervals of constant duration T_{ia} and approximated by a polynomial function f_c of third order in time, which is specified for each x station separately for the ith interval:

$$f_c(x, t) = f_{c0,i}(x) + f_{c1,i}(x)t^* + f_{c2,i}(x)t^{*2} + f_{c3,i}(x)t^{*3} \tag{18}$$

with $t^* = t - t_i$, where $t_i = (i - 1)T_{ia}$ denotes the beginning of the ith interval t_i.

Extensive examinations showed that this function causes only weak oscillations at the freestream boundary in comparison with other functions like higher-order polynomials or trigonometric functions. The coefficients of the polynomial are adjusted after each period i in such a way that the temporal development is continuous up to the second time derivative:

$$f_{c0,i+1}(x) = f_c(x, t_i) \tag{19}$$

$$f_{c1,i+1}(x) = \frac{\partial f_c(x, t_i)}{\partial t} \tag{20}$$

$$f_{c2,i+1}(x) = 0.5\frac{\partial^2 f_c(x,t_i)}{\partial t^2} \tag{21}$$

$$f_{c3,i+1}(x) = -\frac{1}{36T_{ia}^3}\left(6 + 12\frac{\partial}{\partial t} - 11\frac{\partial^2}{\partial t^2}\right) \times [f_c(x,t_{i+1}) - f_{est}(x,t_{i+1})] \tag{22}$$

The estimated values (index $_{est}$) at the end of the following period $i+1$ result from an extrapolation of the temporal development of $\bar{u}_{v,j}(x)$ in the past periods $j \le i$. Equation (22) guarantees that the temporal development of $\bar{u}_v(x)$ is attained exactly after three updates of the coefficients (corresponding to three intervals T_{ia}) if it behaves like a second-order polynomial. We estimate a steady mean in the next period: $f_{est}(x,t_{i+1}) = \bar{u}_{v,i}(x)$ with vanishing time derivatives. This helps to further reduce oscillations of the function f_c.

In our DNS we use time periodic forcing. If the disturbances are periodic with respect to a fixed frequency, here the TS frequency, the mean $\bar{u}_v(x)$ does not vary from one period to the next. Therefore, one period of the forced TS wave T_{TS} is chosen to be the characteristic interval T_{ia} in the interaction model. If the DNS finally gains the desired periodic state, the approximation of the time-averaged influence of the displacement effects upstream of the separation bubble introduces no additional simplifications into the numerical code but, in contrast, removes errors that are generated farther downstream by the modeling of TS waves and vortices with a large amplitude in the interaction model.

For nonperiodic forcing T_{ia} has to be short enough to capture the temporal development of the displacement effects, and a window function (e.g., a Hanning window) can be used to reduce nonperiodic effects. Also overlapping time windows could be helpful.

Downstream of a streamwise station x_{ia} the polynomial function $f_c(x,t)$ and the instantaneous values $u_v(x,t)$ are weighted by means of a blending function $c_i(x)$, which is continuous up to the second x derivative and changes from zero for $x < x_{ia}$ to one for $x > (x_{ia} + \Delta x_{ia})$:

$$[1 - c_i(x)]\, f_c(x,t) + c_i(x)\, u_v(x,t) \tag{23}$$

where Δx_{ia} is approximately one TS wavelength. The position of $x_{ia} + \Delta x_{ia}$ is upstream of the regime of nonlinear disturbance amplitudes to guarantee an instantaneous treatment of such nonlinear TS waves and their higher harmonics at the freestream boundary. Because size and location of the separation bubble may vary during a DNS, x_{ia} is adapted to the flowfield after each interval T_{ia}. Therefore a limit ε_{ia} is introduced, and x_{ia} marks the streamwise station, where the change of the mean $\bar{\boldsymbol{u}}_v(x)$ in the past period exceeds this limit. To place the position $x_{ia} + \Delta x_{ia}$ upstream of the regime with nonlinear TS amplitudes, ε_{ia} has to be comparably small. It was fixed at $\varepsilon_{ia} = 2 \times 10^{-4}$. (This procedure could be improved if ε_{ia} denotes the amplitude where an instantaneous treatment of disturbances at the freestream boundary is required and consequently the blending function is applied upstream of the respective streamwise position.)

Sudden changes of $x_{ia}(t)$ at the step from one TS period to the next are avoided by a smooth temporal adaptation of $c_i(x)$. The computation time for the interaction model is below 1% of the CPU time for the whole numerical scheme.

III. Numerical Test Case

In an experiment performed in the laminar flow wind tunnel of the Institut für Aerodynamik und Gasdynamik, the natural transition in a LSB on a wing section with a chord length of $\hat{c} = 0.615$ m was investigated[24] (no disturbance forcing; TS waves develop from freestream turbulence with $Tu \approx 1.2 \times 10^{-4}$). The freestream velocity $\hat{u}_\infty$ is 29.3 m/s. Accordingly, the chord Reynolds number is $Re_c = 1.2 \times 10^6$. In the DNS the reference length is chosen to be $\hat{L} = 0.0615\,\text{m} = \hat{c}/10$ to obtain length scales between 1 and 10. The resulting Reynolds number in the DNS is $Re = 1.2 \times 10^5$. The nondimensionalized streamwise location $x = 10$ is equivalent to 100% chord, and the DNS chord Reynolds number agrees with the experiment. The integration domain starts at $x = 5$, ends at $x = 10.16$, and the buffer domain at the outflow boundary begins at $x = 9.4$.

In the experiments two velocity distributions $u_p(x)$ at the edge of the boundary layer have been measured. The first one (diamonds in Fig. 1b) refers to a flow with a separation bubble. For the turbulent second one the separation has been suppressed by fixing a turbulator upstream of laminar separation (circles). The difference between the two is caused by displacement effects. Crosses mark the distribution corresponding to the pressure at the wall in the case with separation bubble. To test the interaction model, the turbulent distribution was approximated by a polynomial function (Fig. 1b, solid line) and prescribed as boundary condition u_p in the DNS. If the interaction model works properly, the DNS should finally approximate the experimental conditions with separation bubble (diamonds).

A. Variation of the Height of the Integration Domain

Because the three-dimensional part of the DNS code remained unchanged, extensive two-dimensional simulations were performed to test and validate the numerical model. In five simulations the height of the integration domain was varied between $y_e = 7.29\delta_{1,s}$ (simulation 1) and $19.44\delta_{1,s}$ (simulation 5). For a constant grid spacing ($\Delta y = 0.31$) this corresponds to 145 (simulation 1) and 385 grid points (simulation 5) in the wall-normal direction, respectively. In streamwise direction the grid has 690 points. A TS wavelength is discretized with approximately 40 grid points. In each case the same freestream velocity distribution u_p is prescribed, and a two-dimensional TS wave with an amplitude of $U_{TS} \equiv 10^{-4}$ is forced at the disturbance strip far upstream of the LSB ($5.21 < x < 5.52$).

For the investigation of transition mechanisms, the quality of DNS results mainly depends on an accurate reproduction of the disturbance development. Thus, the independence of the DNS results from the height of the integration domain is evaluated by comparing the amplitude profiles of the forced TS wave U_{TS} and its first higher harmonic U_2 at three streamwise locations in the different integration domains (Fig. 2). To examine the influence of displacement effects on the boundary layer, the mean profiles $\bar{u}$ at the respective positions are also included. At the onset of the adverse pressure gradient, location a, the mean-flow profile has almost Blasius shape, and the TS amplitude of 0.025% is within the linear regime. Consequently, the higher harmonic is negligible [except for the lowest domain (simulation 1), solid line].

At station b the reverse mean-flow velocity near the wall indicates the separation bubble. The potential flow begins at $y/\delta_{1,s} \approx 3.2$. It is significantly accelerated compared to the prescribed potential velocity at this x position, which is included as a vertical line. The deviation declines with increasing wall distance. The TS wave is already strongly nonlinear, and a higher harmonic with large amplitude is present. At the upper boundary of domain 1, the TS wave has an amplitude of almost 1%. Nevertheless, the profile of simulation 1, solid line, fits well with the other simulations. Obviously, the interaction model derives a very accurate boundary condition for TS waves. Behind the LSB (position c) the potential flow is decelerated. The mean-flow profile has an almost turbulent shape because of the saturated TS amplitude. The amplitude and wall-normal extent of the higher harmonic are significantly increased once more. The model predicts correct boundary conditions for disturbance waves even if disturbances with different frequencies and nonlinear amplitude are present at the freestream boundary [in domain 1: $U_{TS}(y_e) \approx 4\%$, $U_2(y_e) \approx 1\%$]. In the three highest domains, 3, 4, and 5, the number of sources in the interaction model was limited to $I = 74$: each TS wavelength is modeled by only five sources; a wavelength of the first higher harmonic covers less than three sources. In simulations 1 and 2 it is twice that number.

The reasons for the slight differences between the computations are now discussed in more detail. Position a is in the region where the temporal behavior at the freestream boundary is approximated by a polynomial function ($x < x_{ia}$) and hence does not allow for oscillations. The fundamental profile U_{TS} in computation 1, solid line, differs from all other simulations, which, in contrast, fit well to each other. The difference is largest near the freestream boundary of integration domain 1. In simulations 2–5 the fundamental wave U_{TS} has a significant amplitude at the wall-normal distance of the freestream boundary of domain 1. In simulation 1 oscillations with fundamental frequency are suppressed, whereas a slow drift is prescribed through the polynomial function, Eq. (18).

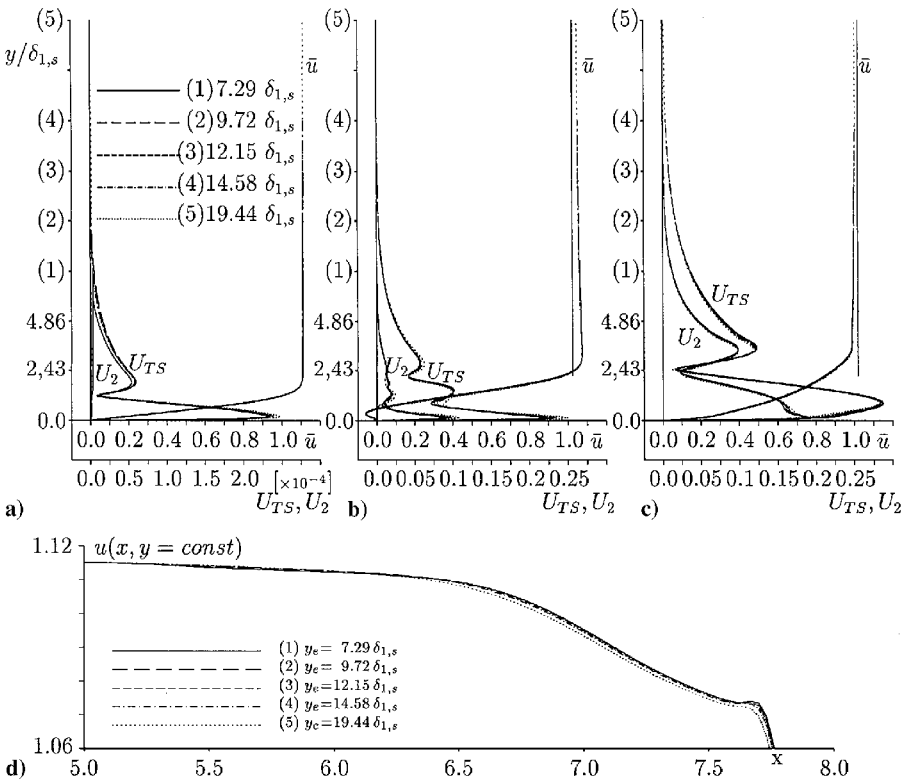

Fig. 2 Comparison of the mean flow $\bar{u}$, the TS wave U_{TS}, and its first higher harmonic U_2 at a) $x = 6.5$, b) $x = 7.7$, and c) $x = 8.0$ in five integration domains with varying height (1)–(5); d) comparison of the respective streamwise velocity component at $y = 3.24\delta_{1,s}$.

Thus, the amplitude in simulation 1 at the freestream boundary represents the Fourier transform of this drift and is not caused by a harmonic oscillation. Thereby, the distribution in a wide range toward the wall is affected, including the second maximum of the TS wave at $y \approx 1.9y/\delta_{1,s}$. Additionally, a higher harmonic U_2 is generated. Prescribing the analytical function, thus may impair the identification of TS waves. The disturbance amplitude $U_{TS} \approx 2.5 \times 10^{-4}$ at location a is very small, and the near-wall maximum agrees well in all computations. Moreover, the further disturbance development is not affected (positions b and c). Nevertheless, domain 1 represents the lower limit for the height of the integration domain because it covers just one boundary-layer thickness at the outflow boundary.

Now we turn our attention to simulation 5, dotted lines, where the disturbance amplitude in the near-wall maximum of the TS wave at positions a and b is approximately 8% larger than in the other computations. Especially at station b), the profiles computed in domain 5 differ slightly from the other simulations. A close-up view on the velocity distribution in the potential flow at a constant distance from the wall (Fig. 2d) explains the differences. In case 5, dotted line, the onset of the strong deceleration and the related higher TS amplification takes place a little further upstream than in the other cases. Namely, the process of disturbance growth and disturbance saturation evolves slightly upstream in comparison with the other cases. Apart from this, the distributions are quite similar. When a state with saturated TS amplitude is once attained in all computations, the differences almost disappear (location c).

Simulation 5 indicates the necessity in very high integration domains to take the inviscid far-away flowfield around the entire airfoil respective within the whole channel into account because in flows with pressure gradient also the streamwise velocity component of the potential flow varies in the y direction. This gradient was neglected in our investigations by prescribing the turbulent velocity distribution measured at a fixed wall-normal distance from the wall in the experiment at different distances in the DNS. However, the wall-normal inviscid velocity component v_p exhibits strong wall-normal gradients even close to the wall resulting in difficulties to define an appropriate Dirichlet boundary condition in the channel formulation (especially in the very common case, when only the wall pressure distribution at the airfoil is known).

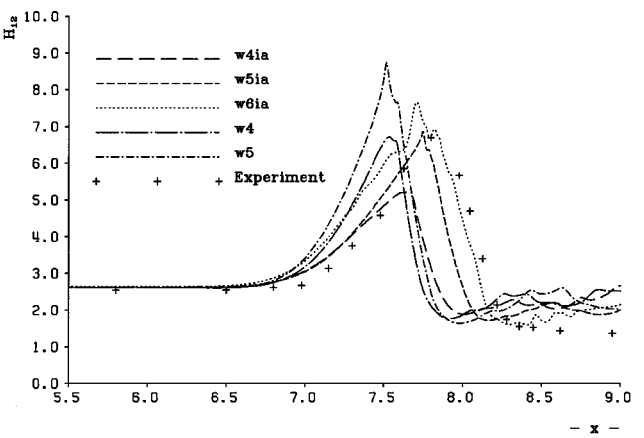

Fig. 3 Comparison of the shape factor from the experiment (symbols) and the DNS.

B. Variation of the Forcing Amplitude

In the underlying experiments neither the exact initial amplitude of the TS waves nor their frequency distribution and spanwise wavenumber spectrum could be determined because the TS amplitude was far below the resolution properties of the hot-wire probe and signal processing used. Before the interaction model was available, the separation bubble in DNS was much shorter than the one observed in the experiments. This was regarded to be caused by different initial conditions of the TS waves, especially different initial amplitudes. Therefore, two-dimensional test calculations were performed, aiming at a coarse fit of the experimental findings by a variation of the initial forcing amplitude in the DNS. However, this attempt failed. The maximum shape factor $H_{12,\max} = 6.75$ agrees well with the experiment (Fig. 3, symbols) if a TS wave with an initial amplitude of $U_{TS} \equiv 10^{-4}$ is forced (case w4, long dash–dotted line). The location of the onset of transition and reattachment in case w4, indicated by the decay of the shape factor, is far upstream compared to the experiment. If the initial amplitude is lowered to $U_{TS} \equiv 10^{-5}$ (case w5, short dash–dotted line), the maximum grows strongly

to $H_{12,\max} = 8.75$, indicating an increased height and reverse-flow intensity in the LSB, but it remains significantly farther upstream than in the experiment.

1. Influence of the Boundary-Layer Interaction

In contrast, with the interaction model applied a reduction of the TS amplitude from 10^{-4} (case w4ia, long dashes), to 10^{-5} (case w5ia, short dashes), and finally 10^{-6} (case w6ia, dots) strongly delays reattachment, and the shape-factor distribution in the separated region tends qualitatively toward the experimental distribution. Downstream of the LSB the experimental results indicate turbulence ($H_{12} \approx 1.5$), whereas the DNS values are significantly higher because of their two-dimensionality. In DNS cases with the same initial TS amplitude, the shape-factor maximum is lower if the boundary-layer interaction is considered. This elucidates the damping influence of displacement effects on the size of the separation bubble.

Time-averaged streamwise velocity fields in the vicinity of the separation bubble without and with interaction model (w5 and w5ia) are plotted in Figs. 4a and 4b, respectively. The isolines $\bar{u} = 0$ are emphasized. Additionally, in Fig. 4b the $\bar{u} = 0$ isoline of case w5 is included to enable a direct comparison of the size and shape of the separation bubble in both cases. The wall-normal direction is stretched by a factor of 20 in comparison with the x coordinate. As just seen, the restrictive boundary condition with neglected interaction effects fixes the separation bubble in streamwise direction.

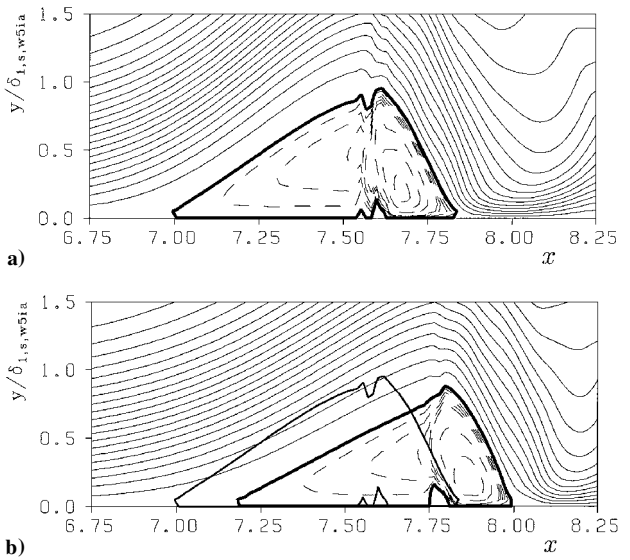

Fig. 4 Isolines of the time-averaged streamwise velocity component $\bar{u}$ a) without (case w5) and b) with (case w5ia) the interaction model, respectively. Lines $\bar{u} = 0$ highlighted. $\bar{u} = -0.2, -0.15, \ldots, 1.0$ and $-0.04, -0.03, -0.02, -0.01$. Negative values dashed.

Thus, the flow separates farther upstream, and the angle of the isoline $\bar{u} = 0$ at separation is larger. The separation bubble is taller, and the reverse-flow velocity maximum is stronger (21% u_∞) than in the case w5ia (19% u_∞).

This is the reason for the higher shape-factor maximum in cases where the boundary-layer interaction is neglected. The shape factor is maximum at the positions $x \approx 7.55$ (w5) and 7.75 (w5ia) in the two cases, which agree with those streamwise positions where the $\bar{u} > 0$ isolines have the biggest distance from the wall, but are different from the streamwise positions with the reverse-flow maximum. The curvature of the isolines in the shear layer in the upstream part of the separation bubbles tends to zero if the interaction model is applied (Fig. 4b). Without the model the curvature is stronger ($x = 6.75 - 7.5$).

2. Comparison with the LST

In Fig. 5 the amplification curves of TS waves for the cases w4, w4ia, w5, and w5ia are shown. For comparison the stability properties of the DNS mean-flow profiles are calculated using the parallel LST, and the respective spatial amplification rates are integrated in streamwise direction (dotted lines). Initially, the amplitude depends only on the forced amplitude. The early deceleration of the potential flow in the cases with interaction model (solid line) soon causes stronger disturbance amplification, and at $x \approx 6.0$ the TS amplitude becomes somewhat larger than in the computations without interaction model (dashed lines). At $x \approx 6.8$ an inverse behavior begins. The disturbance growth in the computations without an interaction model becomes stronger, and at $x \approx 7.0$ the TS amplitude exceeds the amplitude of the respective run applying the interaction model. Finally, the amplitude saturates in both DNS without an interaction model at almost the same streamwise location despite their different initial amplitudes. In contrast, with the interaction model applied wave saturation is delayed if the initial amplitude is decreased. For all cases the agreement between DNS and the parallel LST is very good. Even in the separated region the nonparallel contributions to the stability properties are small, and the assumption of parallel flow in LST is justified.

IV. Transitional LSB

So far, the comparisons between the different DNS aimed at the qualitative understanding of displacement effects. Now, the influence of three-dimensionality is examined by the comparison with the experiment of Würz and Wagner.[24] One would expect that no farther than $x = 7.8$, where the decay of the shape factor in the experiment indicates the onset of transition, three-dimensional modes play an important role and can no longer be neglected. The initially two-dimensional runs w5ia and w6ia, which approximated the experimental shape-factor distributions the best, were continued with a resolution of 44 spanwise spectral harmonics. These runs are marked by the index $_{3D}$. After initial three-dimensional perturbations were excited by pulse-wise forcing in the separation

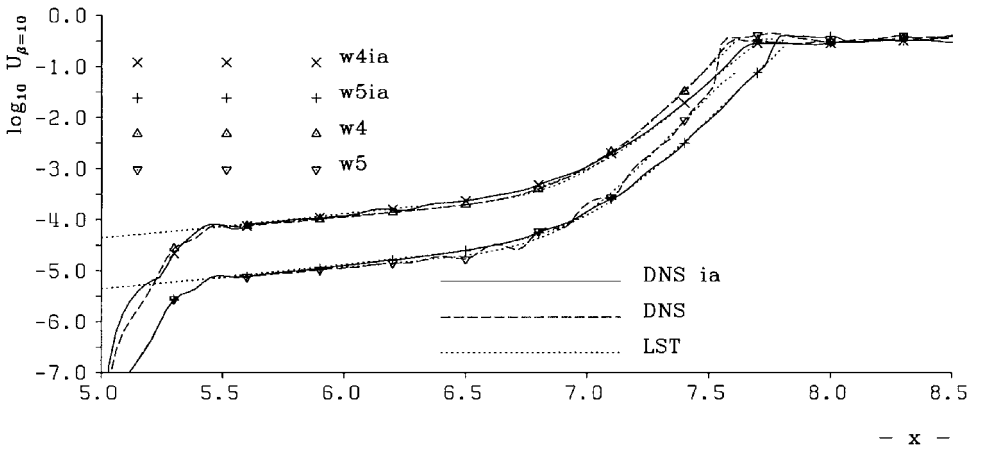

Fig. 5 Amplification of the forced TS wave with the frequency $F = 0.833 \times 10^{-4}$: comparison of DNS (——, with interaction model, and – – –, without interaction model) with linear stability theory (· · ·). $x = 10 \equiv 100\%$ chord length.

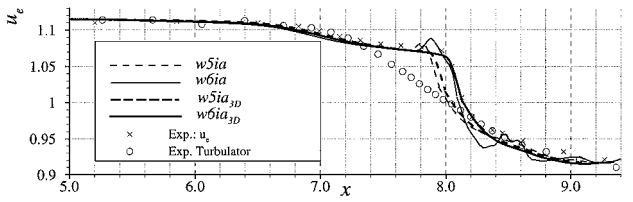

Fig. 6a Comparison of the edge-velocity distributions with interaction considered.

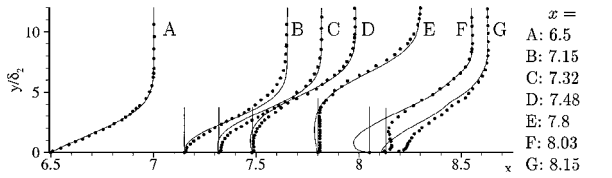

Fig. 6b Case w6ia$_{3D}$: mean-flow profiles at different streamwise stations in comparison with the experiment (symbols).

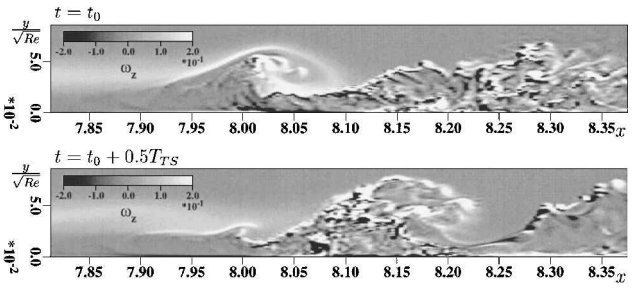

Fig. 6c Case w6ia$_{3D}$: spanwise vorticity ω_z along the centerline ($z = 0$) in the vicinity of reattachment at two time instances separated by one half forcing period T_{TS}.

bubble with very low amplitude, three-dimensional modes start to grow in time (see Ref. 10) and finally transition to turbulence occurs. The edge-velocity distributions in the three-dimensional runs (thick lines in Fig. 6a) deviate in the reattachment region from the respective two-dimensional curves (thin lines), and the overshoot of the velocity distributions observed in the two-dimensional cases upstream of the sudden decay vanishes. Case w6ia$_{3D}$ almost perfectly fits the experiment (×).

Accordingly, the comparison of mean-flow profiles in this case w6ia$_{3D}$ with the experiment (symbols) shows very good agreement for all streamwise stations A–G (Fig. 6b). Initially, the flow is attached (position A). The shear layer then lifts from the wall (B), and the profiles exhibit an inflection point. At station C separation already took place, and a tall reverse-flow region forms (D, E). Finally, a rapid disintegration of the shear layer occurs within only one TS wavelength $\lambda_{TS} \approx 0.3$ (F, G). The differences at the positions F and G near the wall are probably caused by the difficulties in resolving low mean velocities in the experiment with hot wires if the rms amplitude is high. Moreover, at least at position F, the DNS gives evidence for the presence of reverse flow, which cannot be detected by the hot-wires probes either. This causes an underestimation of the shape factor in the experiment, and the shape-factor maximum in the experiment is expected to agree better with case w6ia$_{3D}$ than indicated by Fig. 3.

Figure 6c shows cuts through the instantaneous spanwise vorticity ω_z in the vicinity of reattachment along the centerline of the integration domain at two time instances separated by half a TS forcing period T_{TS}. The flowfield is highly unsteady, and an interpretation of the mean flow is misleading. In particular, no continuous breakdown of the free shear layer and fine-scale turbulence spreading toward the wall and into the potential flow causing reattachment is observed. In contrast, a periodic roll-up of the free shear layer occurs ($t = t_0$, $x = 8.05$). The resulting large-scale vortex starts to propagate downstream and breaks down into fine-scale turbulence ($t = t_0 + 0.5T_{TS}$, $x = 8.15$). Contributions to the understanding of transition or reattachment cannot be expected from the investigation of the time-averaged flowfield. Although the turbulence downstream of the separation bubble (reattachment of the mean flow at $x = 8.15$) is not yet fully resolved and even the three-dimensional DNS results are only of qualitative nature, grid-refinement studies proved that the flow up to the reattachment region is well resolved and the discretization fulfills the requirements to investigate quantitatively the late nonlinear stages of the transition mechanisms involved.

V. Conclusions

Despite big advances in DNS of LSBs in the past 20 years, three-dimensional DNS at large Reynolds numbers as present on high-lift devices or laminar-flow airfoils are just at the very beginning. A major problem is to evaluate a freestream boundary condition if the viscous-inviscid boundary-layer interaction is not negligible. Here, the boundary-layer assumptions are violated, namely the wall-normal pressure gradient deviates from zero. Consequently, a measured pressure distribution (and the respective velocity distribution) at the wall or at the edge of the boundary layer cannot be applied as freestream boundary condition in DNS. Although it is possible to determine the correct distribution iteratively by doing a DNS, comparing the computed pressure distribution with the experiment, correcting the boundary condition, doing the next DNS and so on, this needs tremendous numerical effort and time. Additionally, such DNS depend on reliable measurements with exactly that conditions subject of the DNS investigation (initial disturbances, velocity distribution, etc).

In contrast, if an accurate enough boundary-layer interaction model is applied, DNS can be performed independently from experiments. Only a potential velocity distribution is needed, either calculated with a steady, inviscid numerical scheme or measured in experiments with separation suppressed by a turbulator (thus avoiding strong viscous-inviscid interaction). Comparisons with the experiment are much easier and more essential because the results are not fitted from the beginning by comparisons, but DNS and experiment are independent approaches to the same physical problem. DNS of self-excited transition often suffer from unknown initial conditions (amplitude and character of disturbances in the boundary layer). Without interaction model, agreement with experiments can be strived for by varying the initial conditions or by adapting the freestream velocity distribution. With a model only the influence of the initial disturbance amplitude has to be taken into account.

The application of the interaction model renders fundamental numerical experiments on basic mechanisms in LSBs possible without the necessity of continuous comparisons with measurements. In DNS the initial conditions can be fixed much more easily and accurately than in experiments, which is needed for investigations of interactions of different two- and three-dimensional disturbance waves with low initial amplitude. Thus, DNS can be expected to make large contributions to the understanding of the flow physics of LSBs.

Some of the benefits provided by the interaction model can be gained also without an interaction model by introducing a stretched grid in wall-normal direction outside the boundary layer. However, this reduces the order of accuracy of the numerical scheme and increases errors.

The present model is equally applicable for simulations that take wall-curvature effects into account (in contrast to our current implementation). Otherwise, for the cases described it is advisable to use as low as possible integration domain height to impose the streamwise (inviscid) pressure gradient more accurately on the boundary layer.

Finally and perhaps most importantly, an interaction model is able to catch displacement effects of high-frequency disturbances in the boundary layer and to provide the required instantaneous boundary condition. Consequently, DNS with an interaction model applied can be performed using lower integration domains than without a model.

Acknowledgments

The financial support of the Deutsche Forschungsgemeinschaft under Grant Ri 680/1 is gratefully acknowledged. The authors would like to thank F. R. Hama for the proofreading and his useful comments.

References

[1]Gruber, K., Bestek, H., and Fasel, H., "Interaction Between a Tollmien–Schlichting Wave and a Laminar Separation Bubble," AIAA Paper 87-1256, June 1987.

[2]Gruber, K., "Numerische Untersuchungen zum Problem der Grenzschichtablösung," Ph.D. Dissertation, Univ. Stuttgart, *Fortschritt-Berichte VDI Reihe 7*, VDI-Verlag, Düsseldorf, Germany, 1988.

[3]Pauley, L. L., Moin, P., and Reynolds, W. C., "The Structure of Two-Dimensional Separation," *Journal of Fluid Mechanics*, Vol. 220, 1990, pp. 397–411.

[4]Lin, J. C. M., and Pauley, L. L., "Unsteady Laminar Separation on Low-Reynolds-Number Airfoils," AIAA Paper 93-0209, Jan. 1993.

[5]Ripley, M. D., and Pauley L. L., "The Unsteady Structure of Two-Dimensional Steady Laminar Separation," *Physics of Fluids A*, Vol. 5, No. 12, 1990, pp. 3099–3106.

[6]Rist, U., "Nonlinear Effects of 2D and 3D Disturbances on Laminar Separation Bubbles," *Proceedings of the IUTAM-Symposium on Nonlinear Instability of Nonparallel Flows*, edited by S. P. Lin, Springer-Verlag, New York, 1994, pp. 324–333.

[7]Pauley, L. L., "Response of Two-Dimensional Separation to Three-Dimensional Disturbances," *Journal of Fluids Engineering*, Vol. 116, No. 3, 1994, pp. 433–438.

[8]Rist, U., and Maucher, U., "Direct Numerical Simulation of 2-D and 3-D Instability Waves in a Laminar Separation Bubble," CP-551, AGARD, 1994, pp. 34-1–34-7.

[9]Rist, U., Maucher, U., and Wagner, S., "Direct Numerical Simulation of Some Fundamental Problems Related to Transition in Laminar Separation Bubbles," *Computational Fluid Dynamics '96*, edited by F.-A. Désidéri, C. Hirsch, P. Le Tallec, M. Pandolfi, and F. Périaux, Wiley, New York, 1996, pp. 319–325.

[10]Maucher, U., Rist, U., and Wagner, S., "Secondary Instabilities in a Laminar Separation Bubble," *New Results in Numerical and Experimental Fluid Mechanics*, edited by H. Körner and R. Hilbig, Vol. 60, Vieweg, Brunswick, Germany, 1997, pp. 229–236.

[11]Maucher, U., Rist, U., and Wagner, S., "Transitional Structures in a Laminar Separation Bubble," *New Results in Numerical Fluid Mechanics*, edited by W. Nitsche, H.-F. Heinemann, and R. Hilbig, NNFM Vol. 72, Vieweg, Brunswick, Germany, 1999, pp. 307–314.

[12]Wasistho, B., "Spatial Direct Numerical Simulation of Compressible Boundary Layer Flow," Ph.D. Dissertation, Dept. of Applied Mathematics, Univ. of Twente, Twente, The Netherlands, Dec. 1997.

[13]Alam, M., and Sandham, N. D., "Numerical Study of Separation Bubbles with Turbulent Reattachment Followed by a Boundary Layer Relaxation," *Parallel Computational Fluid Dynamics*, edited by D. R. Emerson, A. Ecer, F. Périaux, N. Satofuka, and P. Fox, Elsevier, Amsterdam, 1998, pp. 571–578.

[14]Spalart, P. R., and Strelets, M. K., "Mechanisms of Transition and Heat Transfer in a Separation Bubble," *Journal of Fluid Mechanics*, Vol. 403, 2000, pp. 329–349.

[15]Alam, M., and Sandham, N. D., "Direct Numerical Simulation of 'Short' Laminar Separation Bubbles with Turbulent Reattachment," *Journal of Fluid Mechanics*, Vol. 403, 2000, pp. 223–250.

[16]Wasistho, B., Geurts, B. J., and Kuerten, J. G. M., "Numerical Simulation of Separated Boundary-Layer Flow," *Journal of Engineering Mathematics*, Vol. 32, 1997, pp. 177–194.

[17]Hsiao, C.-T., and Pauley, L. L., "Comparison of the Triple-Deck Theory, Interactive Boundary Layer Method, and Navier–Stokes Computation for Marginal Separation," *Journal of Fluids Engineering*, Vol. 116, March 1994, pp. 22–28.

[18]Hildings, C., "Simulation of Laminar and Transitional Separation Bubbles," Royal Inst. of Technology, TR-47/19/KTH, Stockholm, Dec. 1997.

[19]Schlichting, H., and Truckenbrodt, E., *Aerodynamik des Flugzeugs*, Springer-Verlag, Berlin, 1959, pp. 391–394.

[20]Veldman, A. E. P., "New, Quasi-Simultaneous Method to Calculate Interacting Boundary Layers," *AIAA Journal*, Vol. 19, No. 1, 1981, pp. 79–85.

[21]Rist, U., and Fasel, H., "Direct Numerical Simulation of Controlled Transition in a Flat-Plate Boundary Layer," *Journal of Fluid Mechanics*, Vol. 298, 1995, pp. 211–248.

[22]Kloker, M., Konzelmann, U., and Fasel, H., "Outflow Boundary Conditions for Spatial Navier–Stokes Simulations of Transitional Boundary Layers," *AIAA Journal*, Vol. 31, No. 4, 1993, pp. 620–628.

[23]Fasel, H., Rist, U., and Konzelmann, U., "Numerical Investigation of the Three-Dimensional Development in Boundary Layer Transition," *AIAA Journal*, Vol. 28, No. 1, 1990, pp. 29–37.

[24]Würz, W., and Wagner, S., "Experimental Investigations of Transition Development in Attached Boundary Layers and Laminar Separation Bubbles," *New Results in Numerical and Experimental Fluid Mechanics*, edited by H. Körner and R. Hilbig, Vol. 60, Vieweg, Brunswick, Germany, 1997, pp. 413–420.

K. Kailasanath
Associate Editor